Thin Solid Films 741 (2022) 139002

Contents lists available at ScienceDirect

Thin Solid Films

journal homepage: www.elsevier.com/locate/tsf

Impact of metallic potassium post-deposition treatment on epitaxial Cu(In, Ga)Se^2

Evandro Martin Lanzoni [*,a], Omar Ramírez [a], Himanshu Phirke [a], Amala Elizabeth [b,c], Harry Mönig [b,c], Alex Redinger [a]

[a] Department of Physics and Materials Science, University of Luxembourg, L-1511, Luxembourg
[b] Westfälische Wilhelms-Universität Münster, Münster 48149, Germany
[c] Center for Nanotechnology (CeNTech), Münster 48149, Germany

ARTICLE INFO

Keywords:
Alkali post-deposition treatment
Copper indium gallium selenide
Solar cells

ABSTRACT

Alkali post-deposition treatments (PDTs) of $Cu(In, Ga)Se^2$ (CIGSe) absorbers are known to improve the power conversion efficiency of the thin-film solar cell devices. The PDTs are usually carried out via evaporation of alkali fluorides in a selenium atmosphere onto a hot substrate. In this work, an alkali metal dispenser was used to evaporate pure metallic potassium onto epitaxial CIGSe absorbers. Subsequently, the absorber layers were heated in-situ to monitor chemical reactions and diffusion into the bulk. Due to the absence of grain boundaries, fluorine, and selenium, the effect of K on CIGSe absorber properties can be directly monitored. We find that potassium effectively diffuses into the bulk of epitaxial CIGSe absorber layers. The diffusion depends on the Cu-content of the CIGSe absorbers, in which Cu-depleted films present higher diffusion rates of K. Photoluminescence (PL) imaging corroborates that K in the bulk of the CIGSe absorber increases the PL yield, suggesting a passivation of defects or an increase in doping. This work highlights that alkali PDTs are not limited by interface and grain boundary modifications but also changes the absorber bulk properties, which needs to be taken into account.

1. Introduction

Over the last years, it has been shown that alkali-metal based post-deposition treatments (PDTs) are an efficient way to improve the optoelectronic properties and thereby the power conversion efficiency of $Cu(In, Ga)Se^2$ (CIGSe) solar cell devices [1–4]. The interplay between the alkali metals, such as Na, K, Rb, Cs, with the polycrystalline CIGSe absorbers is extremely complex and many different observations were reported. On the one hand, it was shown that the CIGSe surface composition changes due to PDTs. A pronounced Cu-depletion was observed and an ion-exchange mechanism was proposed [5]. Furthermore, an alkali containing high bandgap secondary phase was theoretically predicted [6] and sometimes observed at the absorber surface [7–9]. The PDTs with alkali elements are also known to improve the subsequent growth of the CdS buffer layer, which is beneficial for the short circuit current density of the final devices [5].

Other reports show an alkali enrichment at all the interfaces of the CIGSe absorbers, including the grain boundaries [3,10,11] and the back-contact [12]. The accumulation of alkalis at the grain boundaries combined with an increase of the open-circuit voltage suggests efficient grain boundary and interface passivation. This has recently been questioned by Abou-Ras et al. who did not observe improvements in the grain boundary recombination velocities [13]. In addition, a lowering of the Urbach energy due to heavy alkali element treatments was reported, which suggests a modification of the bulk electronic properties [3].

Measurements on CIGSe single crystals (i.e. no grain boundaries) showed that KF PDTs also modified the absorber bulk properties [14]. The KF PDTs improved the quasi-Fermi level splitting in the absorber up to 30 meV, with a strong dependence on the Cu-content. The improvements in quasi-Fermi level splitting after PDTs were attributed to changes in absorber doping.

The majority of the PDTs are based on thermal evaporation of alkali fluorides in a selenium atmosphere onto a heated CIGSe absorber. A comparative study of the standard alkali fluoride and the metallic alkali evaporation PDTs under a Se atmosphere showed a similar beneficial effect on solar cell performance, ruling out a pronounced effect of the fluorine [15]. However, it was shown that selenium PDTs also affects the optoelectronic properties of single-crystalline CIGSe [14]. On top of

* Corresponding author.

https://doi.org/10.1016/j.tsf.2021.139002
Received 18 June 2021; Received in revised form 10 November 2021; Accepted 11 November 2021
Available online 14 November 2021

that, the polycrystalline absorbers exhibit several types of grain boundaries, which may incorporate different amounts of alkali, and consequently, it will generate different degrees of passivation. This claim is supported by Cathodoluminescence measurements that show differences in recombination velocities of approximately two orders of magnitude, depending on the investigated grain [13].

It is therefore, of high importance, to decouple the optoelectronic effect of alkali metals in the CIGSe bulk from the formation of secondary phases at the surfaces and grain boundaries. In this work, pure metallic potassium evaporation on single-crystal CIGSe was carried out in ultra-high vacuum (UHV), followed by a heating step to trigger diffusion and reordering of the alkali elements. The absence of grain boundaries combined with the absence of selenium and fluorine elements during alkali evaporation reduces the formation of alkali metal- and fluorine-rich secondary phases at the interfaces. We combine surface sensitive measurements like Kelvin probe force microscopy (KPFM) and X-ray photoelectron spectroscopy (XPS) with depth profiles measured with secondary-ion mass spectrometry (SIMS), to monitor the presence of K in the absorber. The changes in optoelectronic properties are measured with photoluminescence imaging (PL).

2. Experimental details

2.1. CIGSe growth

Sodium-free single-crystalline CIGSe thin-films were grown by metal-organic vapor phase epitaxy (MOVPE) on (100)-oriented semi-insulating GaAs wafers. Additional information regarding the sample preparation can be found in earlier reports by Ramírez et al. [14], Spindler et al. [16]. The absorber thicknesses were approximately 500 nm and they were transferred via an inert gas transfer system directly into the scanning probe microscopy chamber operated in the low 10^{-10} hPa range. The bulk compositions of the samples were Cu /In = 1.04 (denoted as Cu-rich) and Cu/In = 0.97 (Cu-poor) with similar Ga /(Ga + In) = 0.44, as measured via calibrated energy dispersive X-ray analysis at 10 kV.

2.2. Potassium deposition

Metallic evaporation of potassium was performed in UHV by heating an alkali metal dispenser (supplier: SAES group), which ensures very pure alkali thin-films [17]. A current of 8 A for 10 min was applied to the dispenser for the evaporation, which for our setup resulted in a very thin layer of deposited material. We did not carry out a detailed thickness calibration of the deposited K, a rough approximation will be discussed in the following, which led to a calculated thickness of 8 Å (via Eq. (1)). We stress that this is a rough approximation, but it clearly shows that the deposited amount of K was close to a monolayer before the heat treatment. Subsequently the sample was annealed for 30 min at 200°*C* under UHV conditions. A standard resistive PBN-heater controlled with a TDK-lambda power supply was used for the annealing. With an output power of 9 W, 15 min are needed to reach a sample holder temperature of 200°*C*, which gives an average ramp rate of 11 11°/min. A stable temperature over the 30 min annealing was achieved by reducing the output power to 8 W.

2.3. Characterization methods

Frequency modulation-KPFM measurements were acquired using a UHV variable temperature scanning probe microscope (VT-SPM from Scienta Omicron), where the topography and the workfunction maps were simultaneously measured. Additional protocols can be found in [18]. An AC voltage ranging from 0.2 V to 0.4 V at 1.25 kHz was applied between tip and sample. Pt/Ir PPP-EFM (nanosensors) with a resonance frequency between 70 kHz to 90 kHz were used.

XPS measurements were carried out using a commercial UHV system from SPECS equipped with a PHOIBOS 100 hemispherical analyzer and a delay line detector. A monochromated AlKα X-ray source with a photon energy of 1486.74 eV was used in these measurements. For the XPS, the samples were transferred without air exposure from the VT-SPM to the UHV XPS machine under an inert gas transfer system. From the XPS intensity analysis, the thickness of the deposited K layer can be estimated based on Lambert-Beer's law, which describes the attenuation of the photoelectrons originating from the CIGSe due to an overlayer of K. It can be expressed via

$$I_K = I_0 \cdot \exp\left(-\frac{d}{\lambda_{\mathrm{IMFP}} \cdot \cos\theta}\right) \quad (1)$$

where I_0 and I_K correspond to the peak intensities of the film before and after K deposition. The inelastic mean free path of the photoelectrons penetrating a K overlayer is denoted as λ_{IMFP}, and the angle θ corresponds to the emission angle. We use the intensity changes of the Se3d after K deposition since the binding energy is small, and we do not anticipate strong diffusion due to K deposition. We use calculated values for λ_{IMFP} from the NIST database [19].

SIMS measurements were carried out on absorbers covered with a CdS buffer layer with a Cameca SC-Ultra apparatus. Sputtering was done with Cs^+Cs^+ ions with an energy of 1 keV at 10 nA beam current. All samples were measured in the same measurement session in order to reduce measurement related artefacts.

Photoluminescence imaging was carried out in a custom-built setup that allowed for homogeneous illumination of samples up to an area of 1 × 1 $cm^2 cm^2$ with a pulsed 532 nm laser (Princeton Instruments), equivalent to one sun illumination conditions. The emitted PL signal was collected via an InGaAs-based camera (Xenics) with a high quantum efficiency in the near-infrared. A long-pass filter was used to remove the luminescence originating from the underlying GaAs wafer. The samples were placed inside a sealed box with a glass cover from where the light enters. The sealed box was filled with nitrogen to avoid air exposure.

3. Results and discussions

Fig. 1 (a) depicts KPFM measurements before and after K deposition, according to the recipe described in Section 2. The measurements show facet-related workfunction contrast due to different surface terminations [18,20]. No changes in morphology were visible in the topography images. However, the average workfunction changes substantially from 4.5 eV to 3.5 eV. To corroborate that the lower workfunction is a direct result of the K on the CIGSe surface, XPS measurements were carried out. Fig. 1(b) depicts the measured spectra for the samples before and after K deposition. We observed a clear K2s peak in the spectrum of the K-deposited sample (red) indicating the presence of potassium on the sample surface, whereas the sample prior to the deposition did not show this characteristic peak.

KPFM measurements were used to in-situ monitor changes in the workfunction after each step of the potassium deposition and the subsequent annealings. Fig. 1(c) shows a summary of the average workfunction variations observed during the different steps. The reference workfunction value (red) corresponds to an as-grown sample immediately after transferring it from the MOVPE glovebox to the UHV setup. While keeping the sample under UHV conditions for a period of 20 months, we observed a reduction in the workfunction from 4.63 ± 0.04 eV to 4.39 ± 0.03 eV. We related this change to an accumulation of adsorbates on the sample surface after prolonged exposure to the residual gas atmosphere of the UHV system. We have recently shown that mild annealing of the absorber at 200°*C* allowed us to recover the pristine state of the sample [18]. In accordance with our previous study, the annealing procedure recovered the initial workfunction of the fresh absorber. The subsequent potassium deposition led to a strong reduction of the workfunction (from 4.60 ± 0.06 eV to 3.49 ± 0.06 eV) as already discussed in Fig. 1(a). Such a drastic change was expected, as the

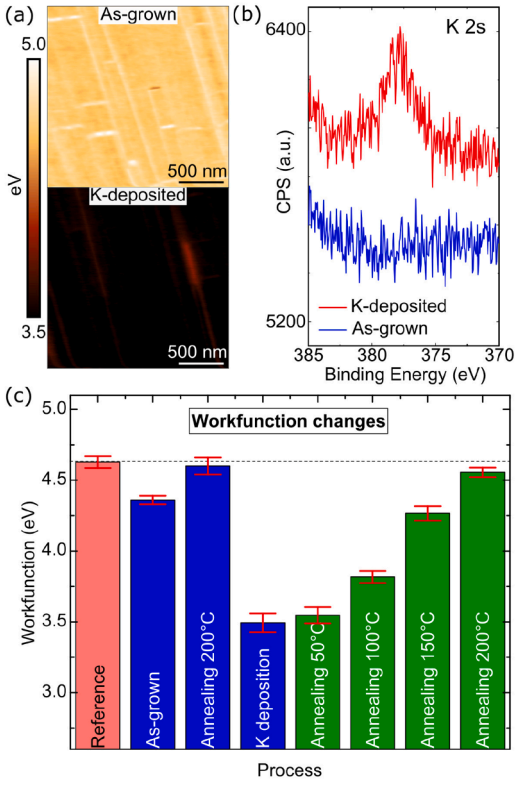

Fig. 1. (a) Kelvin probe force microscopy (KPFM) before and after potassium deposition showing changes in the order of 1 eV in the average workfucntion. (b) X-ray photoelectron spectroscopy (XPS) showing the presence of potassium at the sample surface after deposition. (c) Bar plot summarizing the observed in-situ variations in the workfunction after each step of the potassium deposition. A gradual recovery of the workfunction to the as-grown state is observed after the post-annealing steps.

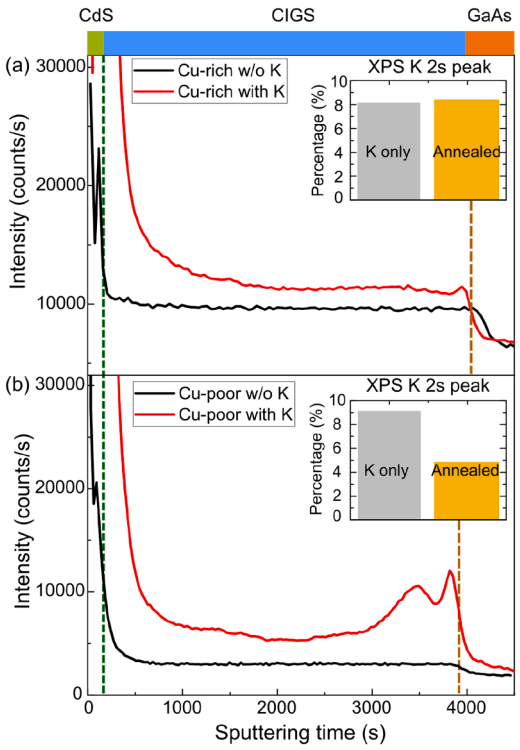

Fig. 2. Secondary-ion mass spectrometry (SIMS) and X-ray photoelectron spectroscopy (XPS) showing the diffusion of potassium in the single-crystal CIGSe (a) Cu-rich and (b) Cu-poor. Red and black curves represent the depth profiles for the annealed samples with and without potassium, respectively. In the Cu-poor case, there is an accumulation of potassium at the interface between CIGSe and GaAs. The insets show the atomic percentage of potassium at the surface of the single-crystal CIGSe measured via XPS, where a reduction to half of the content is showed for the Cu-poor case.

workfunction value for thick potassium films was reported to be 2.74 eV (theoretically) and 2.3 eV (experimentally) [21].

Next, post-deposition UHV annealing steps of 10 min each, ranging from $50^{\circ}C$ up to $200^{\circ}C$, were done. After each annealing step, the average workfunction was measured in order to monitor changes on the CIGSe surface. We observed a gradual recovery of the workfunction (green bars in Fig. 1(c)), indicating a reduction of the K concentration at the surface due to the annealing. After heating to $200^{\circ}C$, the pristine workfunction value was almost recovered.

However, the KPFM measurements did not yield information on the distribution of the K in the bulk after the heat treatments, which is why SIMS measurements were performed on samples with and without K. Fig. 2 depicts the potassium depth profile for the Cu-rich (Fig. 2(a)) and Cu-poor (Fig. 2(b)) annealed samples. In both cases, the red line refers to the depth profile of the sample containing K (plus a post-deposition $200^{\circ}C$ annealing), whereas the black lines arise from samples without K. For the SIMS measurements, the samples had to be air-exposed. Due to the high reactivity of K with moisture, we deposited a CdS buffer layer on top of the CIGSe absorbers via chemical bath deposition. This had the advantage that any residual K on the surface of the CIGSe was removed. The first observation was that we measured a higher amount of K in the K-deposited sample all over the length of the bulk. The initial high K count rate in the CdS layer was observed for all spectra. The reason is not clear at present. However, we note that such high values of K were also observed in other depth profiles [5]. In both samples, we did see an in-diffusion of K into the bulk of the CIGSe. However, for the Cu-poor sample (Fig. 2(b)), we did measure higher count rates in the bulk and a pronounced accumulation at the CIGSe/GaAs interface. The observed double peak at the rear side is probably due to a combination of K accumulation and a change in the matrix (CIGSe versus GaAs). The difference in the K distribution in both films suggested that the diffusion of K in Cu-poor films was easier compared to the Cu-rich films. It was corroborated by XPS measurements (insets of Fig. 2), where the K content at the absorber surface is shown before and after the annealing. The K concentration at the surface did not significantly change for the Cu-rich sample, whereas it drops by half for the Cu-poor case. These results confirmed that K can diffuse in CIGSe absorbers even in the absence of grain boundaries. Furthermore, the diffusion is stronger in the Cu-poor sample, which is probably related to the different amounts of Cu vacancies in both types of absorbers.

Fig. 3 depicts the Cu/(In + Ga), Ga/(Ga + In), and Se/(Cu + Ga + In) ratios at the surface after all the deposition steps, as measured via XPS. In this study, we only focus on relative changes. Consequently, we compare all the surface treatments to the as-grown surface composition ratios. Cu-rich and Cu-poor samples were first UHV annealed, followed by K deposition, and finally, an additional post-deposition UHV annealing of the K-deposited films. Both samples show a pronounced Cu-depletion due to UHV annealing. After K deposition and subsequent annealing, the Cu-ratio decreased even further. For both sets of samples we observed a reduction of approximately 60% compared to the initial state. The Ga/(Ga + In) and Se/(Cu + Ga + In) ratios exhibited less pronounced changes. In addition to the compositional changes, we did not observe strong changes in binding energies. Only a very slightly broadening of the Se 3d peak followed by a small shift in the Se 3d and In 3d peak position that are not strong enough to support the formation of a new chemical bond were observed. We therefore conclude that the only systematic change we observed in XPS was a stronger Cu-depletion due to K, which is inline with the CIGSe literature [5].

Fig. 4 (a) depicts panchromatic PL imaging of the Cu-rich CIGSe

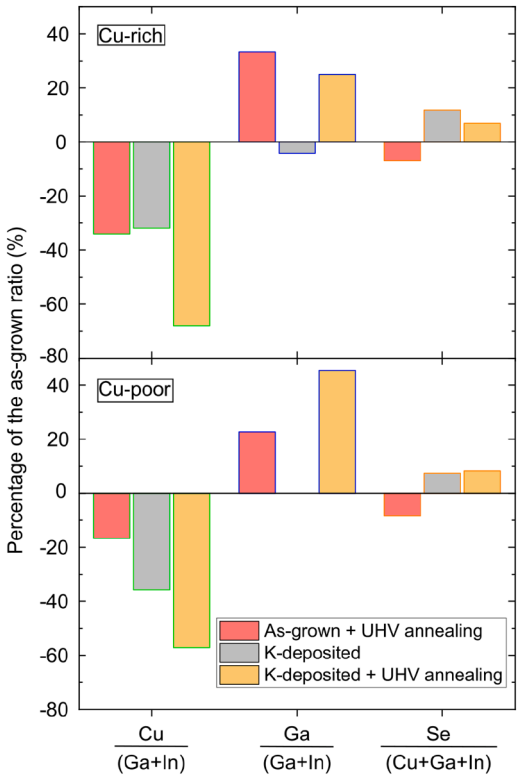

Fig. 3. Changes in the Cu/(Ga + In), Ga/(Ga + In) and Se/(Cu + Ga + In) ratios measured via XPS for the Cu-rich (upper graph) and Cu-poor (bottom graph) samples. The bars represent the changes with respect to the as-grown ratios after each process, as-grown + UHV annealing (red), K-deposited (grey), K-deposited + UHV annealing (yellow). Continuous reduction in the CGI up to 65% is observed. Changes in the Ga, In and Se contents are also observed but it does not follow a trend. (For interpretation of the references to colour in this figure legend, the reader is referred to the web version of this article.)

absorbers. The sample was first UHV annealed to clean the surface, followed by K evaporation and subsequent post-annealing at 200 200°CC. The absorber was then capped with a CdS buffer layer. We did see some rings in the PL intensity image due to optical interference effects of the glass cover of the PL imaging box that was used to measure the samples without air exposure. The rings are therefore not related to the sample and will not be considered in the following. On the K-deposited sample, a region of lower PL yield was observed, which is marked with a dashed blue line in the image. This region was covered with a physical mask that avoided K deposition. The slightly lower PL intensity can also be observed in the line profile presented in Fig. 4(b). Our results suggest that the metallic K deposition followed by annealing has a positive effect on PL yield and therefore on quasi-Fermi level splitting.

Our results are in accordance with the observations of Ramírez et al. [14] for the KF PDTs. The magnitude of the improvement is however different. Whereas Ramírez et al [14]. showed improvements of up to 30 meV after KF treatment, we only measure approximately 2 meV improvement in quasi-Fermi level splitting. The investigated samples however did have different Cu-contents. Comparing samples with similar compositions from Ramírez et al. [14] and this study, the difference in quasi-Fermi level splitting is only 5 meV (7 meV for Ramírez et al. [14]; 2 meV for our study). Moreover, in the present case we evaporated approximately 1 monolayer of K on the CIGSe absorber followed by an in-diffusion step. This is quite different from the Ramírez et al. [14] KF PDTs, which was carried out at higher temperatures and more material (between 6 nm to 10 nm) was evaporated on CIGSe surface during PDTs. Consequently, the observed differences were not

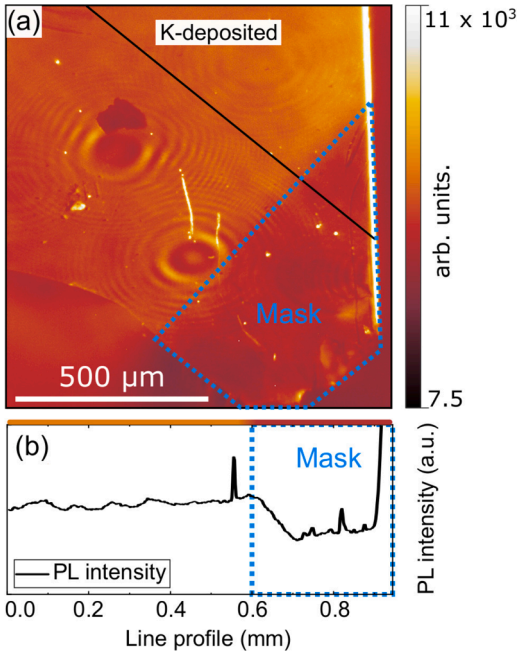

Fig. 4. (a) Photoluminescence (PL) image of the sample with potassium. The dashed blue area is the region where a physical mask was placed over the K-deposited sample. The masked region shows lower PL intensity compared to the area that was exposed to potassium. (b) Line profile (dark line in the image) confirming lower PL intensities at the masked region. (For interpretation of the references to colour in this figure legend, the reader is referred to the web version of this article.)

unexpected. The important point here is that the trend is the same. In order to better compare the results of KF and K deposition, future studies need to be carried out with the same number of K atoms.

4. Conclusions

We have investigated the impact of metallic potassium post-deposition on epitaxially grown Cu(In,Ga)Se^2 absorbers with different integral Cu-contents. We were able to deposit a very thin layer of metallic potassium on the CIGSe sample surface that was annealed to promote diffusion into the absorber. Our KPFM results showed a reduction in the workfunction in the order of 1 eV after potassium deposition, which recovered to the value of the pristine sample after subsequent annealing steps. SIMS depth profiles confirmed that the recovery in workfunction was related to K diffusion into the bulk of the CIGSe absorber even in the absence of grain boundaries. Potassium accumulation at the interface between the CIGSe and the GaAs for the Cu-poor sample indicated a stronger diffusion compared to the Cu-rich sample. The change in diffusion coefficient is most probably related to different amounts of Cu vacancies in the films. XPS measurements supported the SIMS data by showing a reduction in the amount of potassium at the surface after the annealing step for the Cu-poor case, whereas the Cu-rich absorbers did not change within the measurement error. Finally, an improvement in PL intensity was observed for the potassium-treated sample when the same piece of the sample is analyzed via PL imaging. The results highlight the importance of K in the bulk of CIGSe absorbers. The beneficial effect of K cannot be reduced to changes in the grain boundaries in combination with interface passivation. The modification of the CIGSe bulk properties by K (and presumably also by other alkalis) is important too and needs to be analyzed in more detail to fully understand PDTs in CIGSe.

CRediT authorship contribution statement

Evandro Martin Lanzoni: Methodology, Writing – original draft, Writing – review & editing. **Omar Ramírez:** Writing – review & editing. **Himanshu Phirke:** Writing – review & editing. **Amala Elizabeth:** Writing – review & editing. **Harry Mönig:** Supervision, Writing – review & editing. **Alex Redinger:** Conceptualization, Methodology, Supervision, Writing – review & editing.

Declaration of Competing Interest

The authors declare that they have no known competing financial interests or personal relationships that could have appeared to influence the work reported in this paper.

Acknowledgements

The authors acknowledge financial support from the Luxembourg Fonds National de la Recherche (SUNSPOT, Nr. 11244141; "GRISC", Nr. 11696002; and "SeVac" Nr. C17/MS/11655733). AE and HM acknowledge the support by the Deutsche Forschungsgemeinschaft (project number MO 2345/5-1). The authors acknowledge Susanne Siebentritt for the useful discussions, Dr. Conrad Spindler for providing one Cu-rich sample, Dr. Michele Melchirorre for the scanning electron microscopy data, Dr. Nathalie Valle and Brahime El Adib for SIMS measurements and the technicians of the SPM laboratory, Dr. Bernd Uder, Dr. Ulrich Siegel and Nicolas Tournier for technical support.

References

[1] P. Jackson, D. Hariskos, R. Wuerz, W. Wischmann, M. Powalla, Compositional investigation of potassium doped Cu(In,Ga)Se_2 solar cells with efficiencies up to 20.8%, Phys. Status Solidi - Rapid Res. Lett. 8 (3) (2014) 219–222, https://doi.org/10.1002/pssr.201409040.

[2] P. Jackson, R. Wuerz, D. Hariskos, E. Lotter, W. Witte, M. Powalla, Effects of heavy alkali elements in Cu(In,Ga)Se_2 solar cells with efficiencies up to 22.6%, Phys. Status Solidi (RRL) Rapid Res. Lett. 10 (8) (2016) 583–586, https://doi.org/10.1002/pssr.201600199.

[3] S. Siebentritt, E. Avancini, M. Bär, J. Bombsch, E. Bourgeois, S. Buecheler, R. Carron, C. Castro, S. Duguay, R. Félix, E. Handick, D. Hariskos, V. Havu, P. Jackson, H.P. Komsa, T. Kunze, M. Malitckaya, R. Menozzi, M. Nesladek, N. Nicoara, M. Puska, M. Raghuwanshi, P. Pareige, S. Sadewasser, G. Sozzi, A. N. Tiwari, S. Ueda, A. Vilalta-Clemente, T.P. Weiss, F. Werner, R.G. Wilks, W. Witte, M.H. Wolter, Heavy alkali treatment of Cu(In,Ga)Se_2 solar cells: surface versus bulk effects, Adv. Energy Mater. 10 (8) (2020) 1903752, https://doi.org/10.1002/aenm.201903752.

[4] M. Nakamura, K. Yamaguchi, Y. Kimoto, Y. Yasaki, T. Kato, H. Sugimoto, Cd-free Cu(In,Ga)(Se,S)$_2$ thin-film solar cell with record efficiency of 23.35%, IEEE J. Photovoltaics 9 (6) (2019) 1863, https://doi.org/10.1109/JPHOTOV.2019.2937218.

[5] A. Chiril, P. Reinhard, F. Pianezzi, P. Bloesch, A.R. Uhl, C. Fella, L. Kranz, D. Keller, C. Gretener, H. Hagendorfer, D. Jaeger, R. Erni, S. Nishiwaki, S. Buecheler, A. N. Tiwari, Potassium-induced surface modification of Cu(In,Ga)Se_2 thin films for high-efficiency solar cells, Nat. Mater. 12 (12) (2013) 1107, https://doi.org/10.1038/nmat3789.http://arxiv.org/abs/arXiv:1011.1669v3

[6] M. Malitckaya, H.P. Komsa, V. Havu, M.J. Puska, Effect of alkali metal atom doping on the CuInSe_2-based solar cell absorber, J. Phys. Chem. C 121 (29) (2017) 15516, https://doi.org/10.1021/acs.jpcc.7b03083.

[7] N. Taguchi, S. Tanaka, S. Ishizuka, Direct insights into RbInSe_2 formation at Cu(In, ga)Se_2 thin film surface with RbF postdeposition treatment, Appl. Phys. Lett. 113 (11) (2018), https://doi.org/10.1063/1.5044244.

[8] E. Handick, P. Reinhard, R.G. Wilks, F. Pianezzi, T. Kunze, D. Kreikemeyer-Lorenzo, L. Weinhardt, M. Blum, W. Yang, M. Gorgoi, E. Ikenaga, D. Gerlach, S. Ueda, Y. Yamashita, T. Chikyow, C. Heske, S. Buecheler, A.N. Tiwari, M. Bär, Formation of a K-In-Se surface species by NaF/KF postdeposition treatment of Cu(In,Ga)Se_2 thin-film solar cell absorbers, ACS Appl. Mater. Interfaces 9 (4) (2017) 3581–3589, https://doi.org/10.1021/acsami.6b11892.

[9] J. Bombsch, E. Avancini, R. Carron, E. Handick, R. Garcia-Diez, C. Hartmann, R. Félix, S. Ueda, R.G. Wilks, M. Bär, NaF/RbF-treated Cu(In,Ga)Se_2 thin-film solar cell absorbers: distinct surface modifications caused by two different types of rubidium chemistry, ACS Appl. Mater. Interfaces 12 (31) (2020) 34941, https://doi.org/10.1021/acsami.0c08794.

[10] M. Chugh, T.D. Kühne, H. Mirhosseini, Diffusion of alkali metals in polycrystalline CuInSe_2 and their role in the passivation of grain boundaries, ACS Appl. Mater. Interfaces 11 (16) (2019) 14821–14829, https://doi.org/10.1021/acsami.9b02158.

[11] O. Cojocaru-Mirédin, P.P. Choi, D. Abou-Ras, S.S. Schmidt, R. Caballero, D. Raabe, Characterization of grain boundaries in Cu(In,Ga)Se_2 films using atom-probe tomography, IEEE J. Photovoltaics 1 (2) (2011) 207–212, https://doi.org/10.1109/JPHOTOV.2011.2170447.

[12] P. Schoeppe, S. Schoenherr, P. Jackson, R. Wuerz, W. Wisniewski, M. Ritzer, M. Zapf, A. Johannes, C.S. Schnohr, C. Ronning, Overall distribution of rubidium in highly efficient Cu(Ln,Ga)Se_2 solar cells, ACS Appl. Mater. Interfaces 10 (47) (2018) 40592–40598, https://doi.org/10.1021/acsami.8b16040.

[13] D. Abou-ras, A. Nikolaeva, S.C. Dávila, M. Krause, H. Guthrey, M. Al-jassim, M. Morawski, R. Scheer, No evidence for passivation effects of Na and K at grain boundaries in polycrystalline Cu(In,Ga)Se_2 thin films for solar cells, Solar RRL (2019) 1–7, https://doi.org/10.1002/solr.201900095.1900095

[14] O. Ramírez, M. Bertrand, A. Debot, D. Siopa, N. Valle, J. Schmauch, M. Melchiorre, S. Siebentritt, The effect of potassium fluoride postdeposition treatments on the optoelectronic properties of Cu(In,Ga)Se_2 single crystals, Solar RRL 5 (4) (2021) 2000727, https://doi.org/10.1002/solr.202000727.

[15] M. Edoff, T. Torndahl, F. Larsson, O. Stolt, N. Shariati-Nilsson, L. Stolt, Post deposition treatments of (Ag,Cu)(In,Ga)Se_2 thin films for solar cells. Conference Record of the IEEE Photovoltaic Specialists Conference, 2019, pp. 618–621, https://doi.org/10.1109/PVSC40753.2019.8981287.

[16] C. Spindler, F. Babbe, M.H. Wolter, F. Ehré, K. Santhosh, P. Hilgert, F. Werner, S. Siebentritt, Electronic defects in Cu(In,Ga)Se_2: towards a comprehensive model, Phys. Rev. Mater. 3 (9) (2019) 90302, https://doi.org/10.1103/PhysRevMaterials.3.090302.

[17] C. Heske, R. Fink, E. Umbach, W. Riedl, F. Karg, Na-induced effects on the electronic structure and composition of Cu(In,Ga)Se_2 thin-film surfaces, Appl. Phys. Lett. 68 (24) (1996) 3431, https://doi.org/10.1063/1.115783.

[18] E.M. Lanzoni, T. Gallet, C. Spindler, C.K. Boumenou, S. Siebentritt, A. Redinger, O. Ramrez, The impact of Kelvin probe force microscopy operation modes and environment on grain boundary band bending in perovskite and Cu(In,Ga)Se_2 solar cells, Nano Energy 88 (2021) 106270, https://doi.org/10.1016/J.NANOEN.2021.106270.

[19] C.J. Powell, A. Jablonski, NIST Electron Inelastic-Mean-Free-Path Database - Version 1.2, National Institute of Standards and Technology, Gaithersburg, MD, 2010.

[20] E.M. Lanzoni, C. Spindler, O. Ramirez, M. Melchiorre, S. Siebentritt, A. Redinger, Surface characterization of epitaxial Cu-rich CuInSe_2 absorbers. 2019 IEEE 46th Photovoltaic Specialists Conference (PVSC), IEEE, 2019, pp. 2346–2350, https://doi.org/10.1109/PVSC40753.2019.8981200.

[21] N.D. Lang, W. Kohn, Theory of metal surfaces: work function, Phys. Rev. B 3 (1971) 1215–1223, https://doi.org/10.1103/PhysRevB.3.1215.